

Theory of the absorption and circular dichroism spectra of helical molecular aggregates

A. Eisfeld,^{a)} R. Kniprath, and J. S. Briggs

Theoretical Quantum Dynamics, University of Freiburg, Hermann-Herder-Strasse 3, D-79104 Freiburg, Germany

(Received 24 October 2006; accepted 9 January 2007; published online 12 March 2007)

A theory of the electronic circular dichroism (CD) and optical rotatory dispersion (ORD) of infinite aggregates exhibiting cylindrical symmetry is presented in which, to the authors' knowledge, for the first time vibrational structure is included explicitly. It is shown that, with the coherent exciton scattering approximation in the Green function approach, the detailed vibrational structure of the aggregate absorption, CD and ORD bands can be calculated from a knowledge of the electronic coupling and the monomer absorption line shape alone. Detailed model calculations for a single helix are made and the results are used to expose the origin of different spectral features. A good reproduction of experimental *J*-aggregate spectra is obtained, using the same electronic interaction to fit both absorption and CD spectral line shapes. The theory allows some prediction of aggregate geometry to be made, but it is shown that an unambiguous geometrical assignment can only be made where experimental spectra for light of different propagation directions with respect to the cylinder axis are available. © 2007 American Institute of Physics. [DOI: 10.1063/1.2464097]

I. INTRODUCTION

Optical activity is the ability of a medium to rotate plane polarized light and to exhibit different absorption intensities for left and right circularly polarized light. The frequency-dependent difference in absorption of left and right circularly polarized light is called circular dichroism (CD). The frequency-dependent rotation of plane polarized light (which results from the difference in the refractive indices for left and right circularly polarized light) is referred to as optical rotatory dispersion (ORD). Until the beginning of the 1960s, experiments on polymers were restricted almost exclusively to ORD measurements,¹ but now the use of CD has become a standard tool in many areas of physics, chemistry, and biology. As a result of their sensitivity to the molecular geometry, CD and ORD have been utilized for many years to obtain information about molecular structure and the interaction between molecules (e.g., polypeptides and proteins,² chromophores in light harvesting systems,^{3,4} or molecular aggregates⁵). In addition to this classical use of CD, in recent years many new applications have emerged; for example, CD is used to study the chirality of carbon nanotubes⁶ and gold nanoclusters.⁷ An unconventional method based on CD to detect peanut DNA in food by means of a peptide nucleic acid probe and a cyanine dye was suggested,⁸ and it was demonstrated that, with the aid of exciton-coupled CD, DNA can be used as a helical ruler to study the interactions between aligned chromophores.⁹

For a correct interpretation of the measured CD spectra, a good understanding of the origin of optical activity is necessary. An overview of the theoretical description of CD is given, for example, in Refs. 1 and 10–12. An important point to note is that ORD and CD are not independent but are the

real and imaginary parts of the same complex function and are connected by a dispersion relation (in the same way as ordinary dispersion and absorption are connected).

It was realized that even if a molecule does not exhibit optical activity, an aggregate built from such molecules may show strong optical activity (dependent on the arrangement of the molecules). By the term “aggregate” we denote a system composed of molecules (monomers) whose wave functions do not overlap but the monomers interact via transition dipole-dipole forces. It was shown by Kirkwood¹³ how to relate the optical properties of aggregates to the optical properties of the monomers and their interactions. After the discovery of the helical structure of DNA, a lot of work was concerned with (helical) aggregates, e.g., Refs. 14–28.

In his classic paper¹⁴ on the theory of optical activity in long helical aggregates, which is based on the work of Kirkwood,¹³ Moffitt treated the aggregate as a molecular crystal, i.e., periodic boundary conditions were imposed and a Frenkel exciton approach was used to describe the aggregate eigenstates. He used as a starting point for his derivation of optical activity the standard Rosenfeld formalism,²⁹ where it is assumed that the wavelength of light is long compared to the dimensions of the system. In a subsequent publication, Moffitt *et al.*¹⁵ noticed, by considering finite helices without periodic boundary conditions, that an important contribution to the CD (and therefore also to the ORD) spectrum is missing in the treatment of Moffitt. In the late 1960s the origin of the missing term in Moffitt's original treatment was clarified by Ando,³⁰ Loxsom,³¹ and Deutsche.³² It was realized that for long helical aggregates (using periodic boundary conditions), one cannot use the Rosenfeld formalism, but one has to consider the phase variation of the incoming wave over the length of the helix. The connection to polariton modes of molecular crystals was emphasized by Loxsom.³³

^{a)}Electronic mail: eisfeld@physik.uni-freiburg.de

For further reference we summarize briefly the main results of the purely electronic theory of a helical aggregate (using periodic boundary conditions). We follow the development of Mandel and Holzwarth.³⁴ The monomers are labeled with $n=1, \dots, N$, and for each monomer we consider only the ground state (with energy E_0) and the first excited state (with energy E_{mon}). Due to the dipole-dipole interaction between the monomers, in the aggregate the excited state is split into N states with energies given by $E_l = E_{\text{mon}} + C(l)$. In the case of cyclic boundary conditions, the energy shifts with respect to the monomer absorption energy are

$$C(l) = 2 \sum_{n>0} V_{n0} \cos\left(n \frac{2\pi l}{N}\right), \quad (1)$$

where V_{n0} is the interaction energy of monomer n with any fixed monomer (which we take to be the zeroth). For a given orientation of the aggregate with respect to the incoming light beam, only three transitions are allowed. The three excited states reached by these transitions are given by selection rules³²⁻³⁴ $l=Q+N$ and $l=Q \pm M$, where M is the number of turns in the helix and $Q = q_z a N / 2\pi$ (q_z is the projection of the wave vector of the light field onto the helix long axis, which we will just call "the helix axis," and a is the axial translation between neighboring monomers). The corresponding energy shifts $C(l)$ are given by

$$C(l=Q+N) = 2 \sum_{n>0} V_{n0} \cos(nq_z a), \quad (2)$$

$$C(l=Q \pm M) = 2 \sum_{n>0} V_{n0} \cos(n(q_z a \pm \phi)). \quad (3)$$

Here ϕ is the azimuthal rotation angle between neighboring monomers. For light propagating perpendicular to the helix axis ($q_z=0$ and therefore also $Q=0$), transitions are allowed to states with $l=N$ and $l=\pm M$. This situation is sketched in Fig. 1(a). The transition from the ground state to state $l=N$ has an electronic transition dipole which is polarized parallel to the helix axis. The two degenerate states $l=\pm M$ both have an electronic transition dipole oriented perpendicular to the helix axis. The total CD belonging to these two bands has the same strength as, but opposite sign compared to, the CD band with $l=N$ (see, e.g., Refs. 32 and 33). By contrast, for light propagating along the helix axis ($q_z \neq 0$ and therefore $Q \neq 0$), transitions are electric dipole allowed only to states with $l=Q \pm M$ [see Fig. 1(b)]. The CD of the $l=Q+M$ state has equal magnitude but opposite sign compared to the $l=Q-M$ state. The treatment of Moffitt formally corresponds to setting $Q \equiv 0$. Then the energetic splitting of the two levels vanishes and the CD signals belonging to these levels cancel each other identically.

From the foregoing one sees that it is convenient to distinguish the propagation direction of the incoming light and the polarization with respect to the helix axis. We will denote properties obtained for light propagating parallel (perpendicular) to the helix axis with a superscript para (perp). With a subscript \parallel (\perp) we denote linear polarization parallel (perpendicular) to the helix axis.

Initially, the study of helical aggregates was mainly devoted to polypeptides, but there has been a growing interest

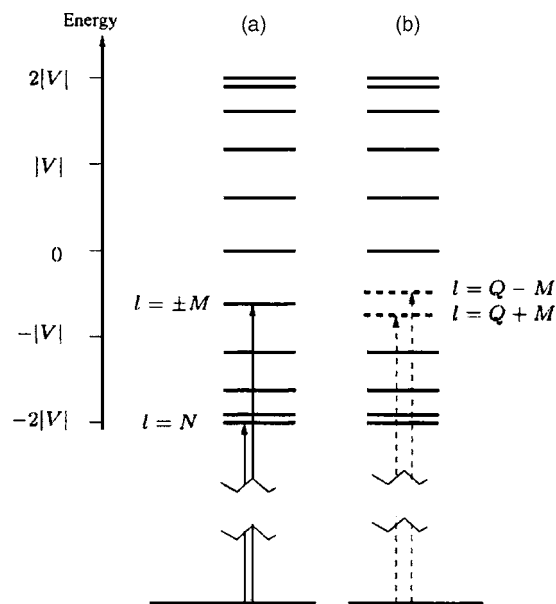


FIG. 1. The eigenenergies and allowed optical transitions of a helical aggregate consisting of $N=20$ monomers and 5 monomers per turn (cyclic boundary conditions and nearest-neighbor couplings are used; the interaction energy between neighboring monomers is denoted by V and is taken to be negative). The monomer excited energy is taken to be the zero of energy. (a) Light propagating perpendicular to the helix axis. (b) Light propagating parallel to the helix axis.

in helical and cylindrical aggregates composed of organic dyes.³⁵⁻⁴⁷ These dyes spontaneously self-assemble in solution or on DNA nanotemplates. In several light harvesting systems, one has found a cylindrical arrangement of the porphyrines⁴⁴ and it is suggested that organic dye aggregates are promising candidates for the study of artificial light harvesting.⁴³ In recent years it became also possible to resolve the structure of certain molecular aggregates consisting of organic dyes on the nanoscale using cryogenic temperature transmission electron microscopy (cryo-TEM),^{48,49} and a cylindrical structure of these aggregates was proposed.⁴⁷

As a result of the growing interest in these structures, we will investigate in this work the absorption and the CD spectra of cylindrical aggregates. Helical aggregates, linear stacks, and aggregates in the form of a ring are special cases of this geometry. In the monomer spectrum these dyes show pronounced broadening of the electronic transition due to internal vibrations and coupling to the environment. Therefore, a theory which describes the absorption line shape and the line shape of the CD spectrum has to take care of these effects. There have been different approaches to the inclusion of vibrations (e.g., Refs. 50-52) and various kinds of disorder (e.g., Refs. 53-57) into the simple Frenkel exciton model. One of these approaches is the coherent exciton scattering (CES) approximation, which was developed to include internal vibrations^{52,58} and later extended to include also various other mechanisms responsible for spectral broadening.⁵⁷ In previous publications^{57,59,60} we investigated the absorption spectra of molecular aggregates consisting of organic dyes using the CES approximation and found very good agreement between theory and experiment. The main idea behind the CES approach is to calculate the absorption spectrum of the aggregate using the measured (or calculated)

absorption spectrum of the monomers. Here we will develop this approach further and apply it to the calculation of aggregate CD spectra. The monomers of the dyes considered in this work do not exhibit CD, so that the observed CD of the aggregate is solely due to the geometrical arrangement and the interaction between the constituent monomers.

The paper is organized as follows: In Sec. II we give an introduction to the theoretical treatment of optical activity of long aggregates and a short review of the CES approximation. Then in Sec. III the formulas for absorption and CD within the CES approximation are presented and discussed. After that we illustrate the predictions of the CES theory by specific examples of helical aggregates with varying arrangements of the monomers. In Sec. IV we compare with experimental spectra of dye aggregates. Section V contains a discussion of the results and an outlook.

II. ABSORPTION AND CD IN THE CES APPROXIMATION

A. General formalism

Consider an aggregate of arbitrary geometry. The position of the n th monomer is denoted by X_n and its electronic transition dipole is μ_n . We assume that the distance between the monomers is so large that there is essentially no overlap of electronic wave functions of different monomers. The monomers interact via transition dipole-dipole forces. The aggregate Hamiltonian H can be written as $H=H_0+V$, where H_0 is the Hamiltonian of the noninteracting monomers and V is the interaction. The Green operators of the monomers and the aggregate are denoted by

$$g(E) \equiv (E - H_0 + i\delta)^{-1}, \quad (4)$$

$$G(E) \equiv (E - H + i\delta)^{-1} = (E - (H_0 + V) + i\delta)^{-1}, \quad (5)$$

respectively. Note the identity

$$\frac{1}{E - H + i\delta} = \frac{1}{E - H_0 + i\delta} + \frac{1}{E - H_0 + i\delta} V \frac{1}{E - H + i\delta} \quad (6)$$

or

$$G = g + gVG. \quad (7)$$

This identity, which is extensively used below, is easily proved by multiplying Eq. (6) from the right by the operator $E - H + i\delta$.

Since the Green operator is directly related to the absorption spectrum [see Eq. (10)] and the Green operator of the aggregate $G(E)$ is connected with that of the noninteracting monomers $g(E)$ via the identity Eq. (7), this approach is well suited to express the aggregate absorption (and CD spectrum) as a function of the monomer absorption spectrum and the interaction V (see, e.g., Ref. 58).

In the following we take the electronic and nuclear motions in the monomers to be Born-Oppenheimer separable. Furthermore, we consider only the electronic ground state and one single electronic excited state.

The electric field (at position x and at time t) of the incoming light wave with frequency ω and with wave vector q is given by

$$E(x, t) = \text{Re}\{\mathcal{E}e^{i(qx - \omega t)}\}. \quad (8)$$

The field strength can be written as $\mathcal{E} = \epsilon|\mathcal{E}|$, where the complex unit vector ϵ gives the polarization of the electric field. A complex value of ϵ corresponds to elliptically polarized light, e.g., for a light wave traveling in the positive z direction, the choice $\epsilon = (1/\sqrt{2})(\hat{e}_x - i\hat{e}_y)$ leads to an electric field that rotates in a clockwise sense as viewed by an observer facing the negative z direction (he/she is looking at the source). Light with this behavior will be called right circularly polarized. If $\epsilon = (1/\sqrt{2})(\hat{e}_x + i\hat{e}_y)$, the light is said to be left circularly polarized.

Because the size of a monomer is small compared to the wavelength of the light, one can assume that the electric field of the light wave is constant over one monomer. However, note that the phase variation of the field over the whole extent of the aggregate will be retained. As outlined in Sec. I this is necessary when the aggregate size along the direction of light propagation is not small compared to the wavelength of the light. Then the interaction of the incoming light with the aggregate can be written

$$U(t) = - \sum_n \mu_n \cdot E(X_n, t). \quad (9)$$

The aggregate is initially in its ground state, which means that all monomers are in their electronic ground state and also in the vibrational ground state. By the same procedure as used in Ref. 58, the aggregate absorption cross section for light with energy $\hbar\omega$, wave vector q , and polarization ϵ can be written as

$$\sigma_q^\epsilon(\omega) = - \frac{4\pi}{c} \omega \text{Im} \sum_{nm} (\epsilon^* \cdot \mu_n) e^{-i(q \cdot X_n)} \times \langle G_{nm}(\omega) \rangle e^{i(q \cdot X_m)} (\mu_m \cdot \epsilon). \quad (10)$$

Here c is the velocity of the light and $G_{nm}(\omega) \equiv \langle \pi_n | G(E_0 + \hbar\omega) | \pi_m \rangle$, where $|\pi_m\rangle$ denotes a state in which monomer m is electronically excited and all others are in their electronic ground state. The brackets $\langle \cdot \cdot \rangle$ in Eq. (10) denote an average over the vibrational ground state and $\omega = (E - E_0)/\hbar$. As shown in Ref. 57 in the same way it is possible to treat also finite temperature and the influence of different kinds of disorder.

Let $\sigma_q^{L/R}(\omega)$ denote the absorption of left/right circularly polarized light that is propagating in the direction of q . Then one can write the CD for light propagating in direction q as

$$\text{CD}_q(\omega) = \sigma_q^L(\omega) - \sigma_q^R(\omega). \quad (11)$$

Equations (10) and (11) are our basic formulas. As already mentioned ORD can be obtained from the CD by use of a Kramers-Kronig transformation.¹²

B. The CES approximation in the Green function approach

The fundamental equation [Eq. (10)] is expressed in terms of the aggregate Green operator $G(E)$. To obtain the monomer absorption spectrum, one simply replaces G_{nm} in Eq. (10) by $g_n \delta_{nm}$, where $g_n = \langle \pi_n | g | \pi_n \rangle$. Note that g_n and G_{nm} are still dependent on nuclear coordinates. To find a

connection between the monomer absorption spectrum and the aggregate absorption spectrum, we use the definitions Eqs. (4) and (5). Taking matrix elements of Eq. (7) in the $|\pi_n\rangle$ basis [the states $|\pi_n\rangle$ are defined after Eq. (10)] and averaging over the ground vibrational state we obtain

$$\langle G_{nm} \rangle = \langle q_n \rangle \delta_{nm} + \sum_{n'} \langle g_n V_{nn'} G_{n'm} \rangle. \quad (12)$$

In the CES approximation^{57,58} the monomer Green operator g_n is replaced by its average $\langle g \rangle$, which is independent of n for identical monomers. This leads to the equation

$$\langle G_{nm} \rangle = \langle g \rangle \delta_{nm} + \langle g \rangle \sum_{n'} V_{nn'} \langle G_{n'm} \rangle, \quad (13)$$

which will be used to obtain the absorption and CD spectra. Because $\langle g \rangle$ as well as $\langle G \rangle$ are complex quantities, their knowledge not only gives the absorption and CD (which are proportional to the imaginary part), but also the dispersion and the ORD (which are proportional to the real part).

III. RESULTS

In this section the general approach of the previous section is applied to the special case of an infinite cylindrical aggregate. The arrangement of the monomers is sketched in Fig. 2. As discussed in Ref. 46 the cylindrical aggregate can be viewed as composed of several helices wound around the surface of the cylinder. However, the analysis for several helices wound around a cylinder is valid also for a single helix and even applies when the radius of the helix shrinks to zero. We consider \mathcal{N}_2 identical helices with helicity angle ϕ_1 (see Fig. 2). The separate helices (in Fig. 2, six in total) are rotated through an angle ϕ_2 with respect to each other so that $\phi_2 = 2\pi/\mathcal{N}_2$. Then the monomers are arranged in an infinite cylindrical stack of circular rings of \mathcal{N}_2 monomers. An individual ring is denoted by n_1 , and the monomers within one ring are labeled by n_2 . Each monomer is then labeled by (n_1, n_2) , with $-\infty \leq n_1 \leq \infty$ and $0 \leq n_2 < \mathcal{N}_2$. It will be convenient to use the short notation $\mathbf{n} \equiv (n_1, n_2)$, $\boldsymbol{\phi} \equiv (\phi_1, \phi_2)$, $\mathbf{n}\boldsymbol{\phi} = n_1\phi_1 + n_2\phi_2$. Let ρ denote the radius of the cylinder/helix (which is assumed to be much smaller than the wavelength of the incoming light) and a the distance between neighboring rings. The radial, tangential, and vertical (parallel to the helix axis) components of the transition dipoles of the monomers are given by $\mu_r \equiv \mu \sin \beta \sin \alpha$, $\mu_t \equiv \mu \sin \beta \cos \alpha$, and $\mu_v \equiv \mu \cos \beta$ [with α and β as defined in Fig. 2(a)]. For a more detailed discussion of the cylinder geometry, see Appendix A.

The further results presented in this section are derived in detail in Appendix B. There one sees that it is convenient to define an aggregate line shape function

$$S(C, \omega) \equiv -\text{Im} \frac{\langle g(\omega) \rangle}{1 - C \langle g(\omega) \rangle}, \quad (14)$$

where C is a real number with dimension of energy and Im denotes the imaginary part. It is important to note that for a given monomer line shape function $-\text{Im}\langle g(\omega) \rangle$, the aggregate line shape function $S(C, \omega)$ depends only on the value of C , since $\text{Re}\langle g(\omega) \rangle$ can be obtained from a Kramers-Kronig

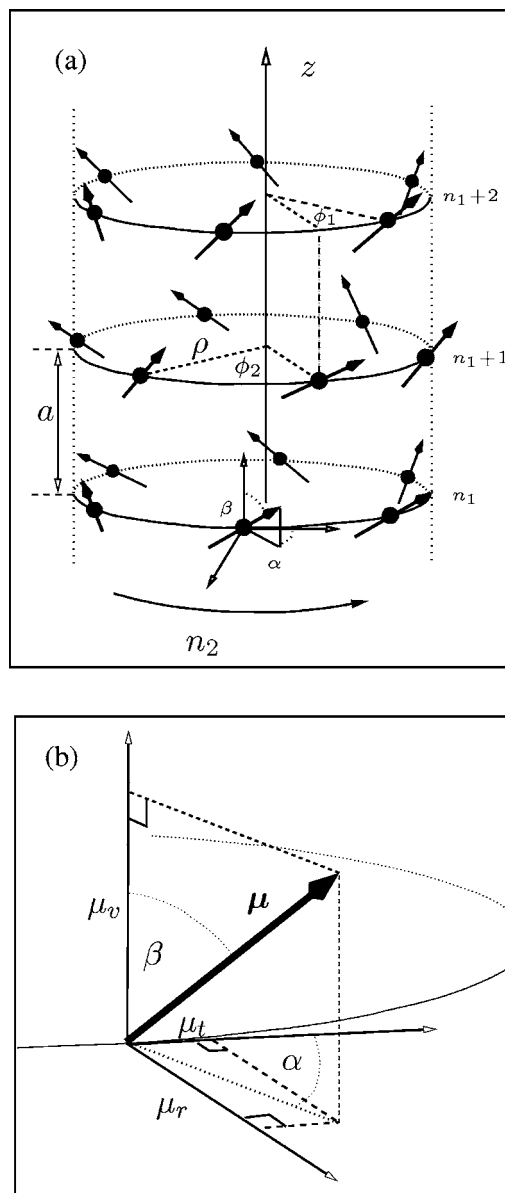


FIG. 2. The cylindrical geometry showing (a) the positions of the monomers and (b) the components of the monomer transition dipoles.

transform. Furthermore, the center (first moment) of $S(C, \omega)$ is shifted by the energy C with respect to the center of the monomer absorption line shape $-\text{Im}\langle g(\omega) \rangle \equiv S(0, \omega)$ and the integrated area $\int S(C, \omega) d\omega$ is independent of the value of C (this follows directly from the sum rules discussed in Ref. 58). In the following the ω dependence of $S(C, \omega)$ is not written explicitly anymore.

A. Absorption

For light propagating perpendicular to the cylinder axis, one finds an absorption cross section

$$\sigma^{\text{perp}} = \frac{4\pi N}{c} \omega^2 \left(\frac{(\mu_r^2 + \mu_t^2)}{2} S(C_{\perp}) + \mu_v^2 S(C_{\parallel}) \right). \quad (15)$$

For light propagating parallel to the helix axis, the absorption cross section is

$$\sigma^{\text{para}} = \frac{4\pi N}{2c} \omega \left(\frac{(\mu_r^2 + \mu_t^2)}{2} \right) (S(C_L) + S(C_R)). \quad (16)$$

The interaction energies C_{\parallel} , C_{\perp} , and $C_{R/L}$ are given by

$$C_{\parallel} = \sum_n V_{n0}, \quad (17)$$

$$C_{\perp} = \sum_n \cos(n\phi) V_{n0}, \quad (18)$$

$$C_{R/L} = \sum_n \cos(n\phi \mp n_1 a q) V_{n0}, \quad (19)$$

where V_{n0} denotes the interaction of monomer n with the monomer labeled 0 . Since the V_{nm} are assumed independent of vibrations, these energies (C_{\parallel} , C_{\perp} , and $C_{R/L}$) are just the energy shifts from the monomer excited-state energy which would occur in a purely electronic theory of absorption. In the case of a helix, which was discussed in Sec. I, the energies C_{\parallel} , C_{\perp} , and $C_{R/L}$ correspond to $C(l=N)$, $C(l=M)$, and $C(l=Q \pm M)$, respectively [see Eqs. (2) and (3)]. In Eq. (22) the contribution proportional to μ_v^2 stems from light polarized parallel and the contribution proportional to $\mu_r^2 + \mu_t^2$ from light polarized perpendicular to the cylinder axis. In the case of light propagating parallel to the cylinder axis [Eq. (23)], the polarization is perpendicular to the cylinder axis.

If $|C_{\perp} - C_{L/R}|$ is small compared to the width of $S(C_{\perp})$, which will be the case for $aq \ll 1$, the absorption cross section for light propagating parallel to the helix axis can be written

$$\sigma^{\text{para}} \approx \frac{4\pi N}{c} \omega \left(\frac{(\mu_r^2 + \mu_t^2)}{2} \right) S(C_{\perp}). \quad (20)$$

In the case of an isotropic ensemble of aggregates (denoted by ^{iso}), one then obtains

$$\begin{aligned} \sigma^{\text{iso}} &= \frac{1}{3} (\sigma^{\text{para}} + 2\sigma^{\text{perp}}) \\ &\approx \frac{4\pi N}{3c} \omega ((\mu_r^2 + \mu_t^2) S(C_{\perp}) + \mu_v^2 S(C_{\parallel})). \end{aligned} \quad (21)$$

B. Circular dichroism

The CD signal for light propagating perpendicular to the cylinder axis is given by

$$\text{CD}^{\text{perp}} = \frac{4\pi N}{c} \omega \mu_r \mu_v \frac{2\pi\rho}{\lambda} (S(C_{\parallel}) - S(C_{\perp})), \quad (22)$$

where $\lambda = 2\pi c/\omega$ denotes the wavelength of the light. This shows that for light propagating perpendicular to the helix axis, the CD spectrum consists of two bands with opposite sign and equal strength [see the discussion after Eq. (14)]. The line shapes of the two bands are identical to the corresponding line shapes of the absorption bands for light that is polarized parallel or perpendicular to the helix axis, respectively. The magnitude of the signal is proportional to the cylinder radius ρ and to the vertical and tangential components μ_v , μ_t of the monomer transition dipoles.

The CD signal for light propagating parallel to the cylinder axis is given by

$$\text{CD}^{\text{para}} = \frac{4\pi N}{c} \omega \frac{(\mu_r^2 + \mu_t^2)}{2} (S(C_L) - S(C_R)). \quad (23)$$

Note that in contrast to Eq. (22) the dimensionless ratio ρ/λ does not occur. In the case of an isotropic sample, one has

$$\text{CD}^{\text{iso}} = \frac{1}{3} (\text{CD}^{\text{para}} + 2\text{CD}^{\text{perp}}). \quad (24)$$

If the distance a is much smaller than the wavelength of light, Eq. (23) can be approximated by (see Appendix B)

$$\begin{aligned} \text{CD}^{\text{para}} &\approx \frac{4\pi N}{c} \omega (\mu_r^2 + \mu_t^2) \frac{2\pi a}{\lambda} \\ &\times \left[\sum_n n_1 \sin(n\phi) V_{n0} \right] \frac{\partial}{\partial(\hbar\omega)} S(C_{\perp}), \end{aligned} \quad (25)$$

which shows that the line shape of the CD band is approximately the derivative of the corresponding absorption line shape $S(C_{\perp})$ for light polarized perpendicular to the helix axis. In this approximation a factor a/λ appears in Eq. (25) in analogy to the factor ρ/λ in Eq. (22). The expression Eq. (25) is essentially that given by Moffitt *et al.*¹⁵ as the missing term in Moffitt's¹⁴ work. This term also appears in the recent work of Didraga *et al.*⁴⁶ on cylindrical aggregates. However, one sees that Eq. (25) is an approximation to the exact result of Eq. (23). Note also that in our approach the line shape $S(C_{\perp})$ is not introduced as a line broadening at the end of the calculation as, for example, in Ref. 46, but is decided explicitly by the monomer line shape and the interaction energy C_{\perp} .

By comparing Eqs. (23) and (22), one sees that the orientation of the monomers with respect to the helix axis plays a crucial role in deciding the magnitudes of CD^{para} and CD^{perp} . Consider, for example, the extreme cases when either CD^{para} or CD^{perp} vanishes identically. From Eq. (22) one sees that CD^{perp} vanishes if either the tangential component μ_t or the vertical component μ_v of the transition dipoles of the monomers is zero. On the other hand [see Eq. (23)], CD^{para} only vanishes if both μ_r and μ_t are zero (which means that all transition-dipole moments are aligned parallel to the cylinder axis). This implies that when CD^{para} vanishes, CD^{perp} vanishes also. In addition, the absorption cross section for light polarized perpendicular to the helix axis vanishes also [see Eqs. (15) and (16)].

In Refs. 61 and 62 it is shown that if one starts with the Rosenfeld formalism within the framework of the CES approximation, one only obtains the contribution CD^{perp} .

C. An example calculation

To illustrate the use of the CES method, we will consider a helical aggregate composed of identical monomers and investigate the dependence of the absorption, CD, and ORD spectra on the number of monomers per helix turn. Since we are dealing with a single helix (and not a cylinder), there is only one monomer per ring in Fig. 2 and therefore only the angle $\phi \equiv \phi_1$ has to be considered. Note that the number of

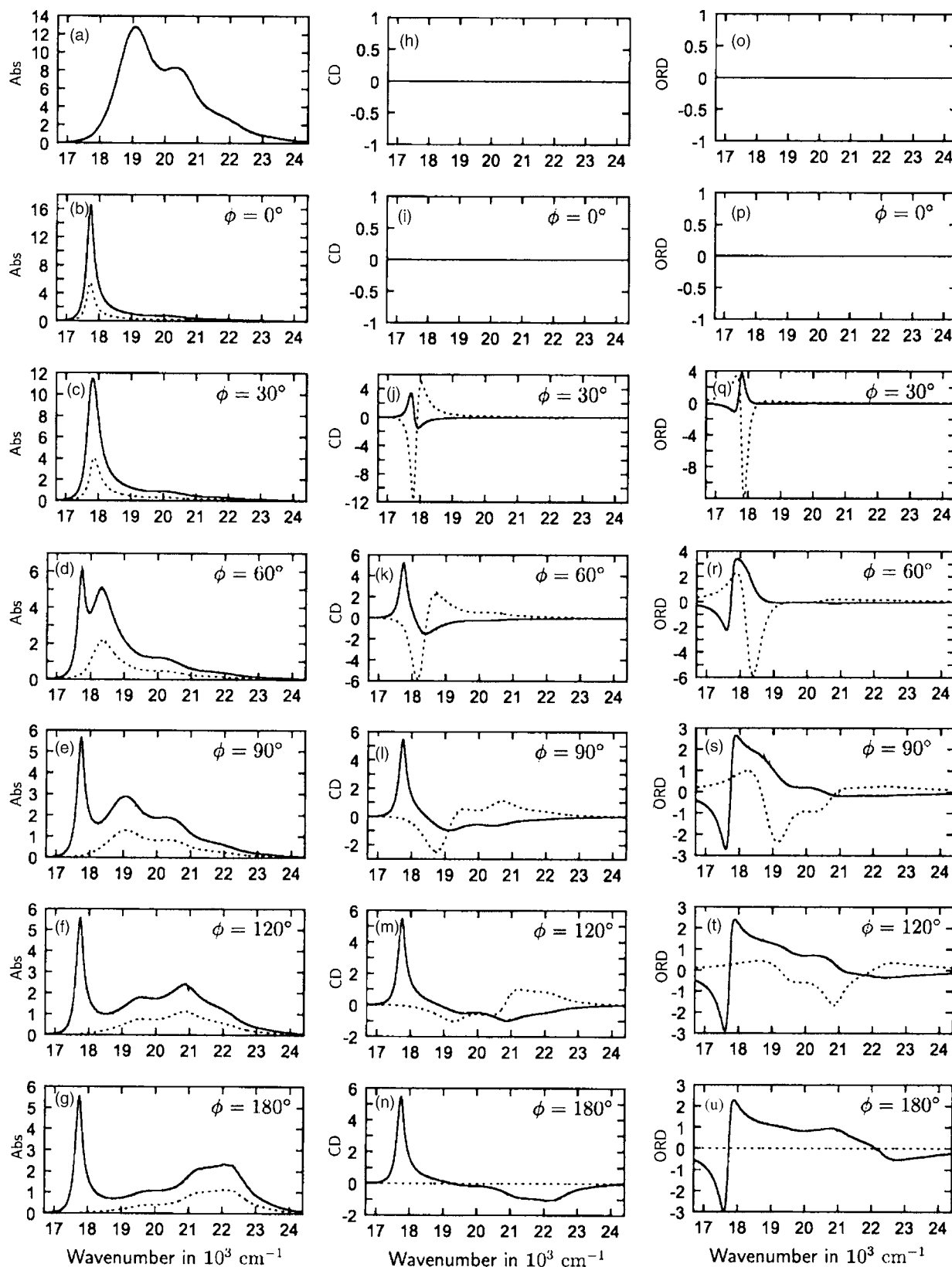


FIG. 3. Aggregate absorption, CD, and ORD spectra for different angles ϕ : left column, absorption; middle column, CD; and right column, ORD. For details see text. Upper row: monomer-spectra ($V=0$). All other spectra are calculated with $V=-750\text{ cm}^{-1}$ and given in arbitrary units.

monomers per turn determines the angle ϕ . For the absorption spectrum of the monomers, we take as example a typical spectrum of an organic dye, specifically the monomer absorption spectrum of the pseudoisocyanine (PIC) dye mea-

sured in Ref. 63. This monomer absorption line shape is shown in Fig. 3(a). Note that the monomer absorption is proportional to $-\text{Im}\langle g(\omega) \rangle$. The real part of $\langle g(\omega) \rangle$ can then be calculated using a Kramers-Kronig relation. The (com-

plex) function $\langle g \rangle$ so obtained is inserted in Eqs. (15) and (16) to give the aggregate absorption spectrum and in Eqs. (22) and (23) to give the CD spectrum. The PIC monomer possesses no intrinsic CD or ORD [see Figs. 3(h) and 3(o)].

To calculate the aggregate spectra, one has to specify details of the geometry of the helix (see Fig. 2). The axial translation between neighboring monomers is taken to be $a = 1$ nm, which is roughly the order of magnitude one expects from cryo-TEM measurements.^{48,49} The absorption spectrum covers the spectral range from $\lambda = 400$ nm to $\lambda = 600$ nm. Therefore the product aq is of the order of 1/100 and we have used that value in the calculations [note that for $aq = 1/100$ the approximate equations (21) and (25) are valid and a only scales the magnitude of CD^{para}].

Since in the following calculations the focus lies on the line shape of the spectra (and not on their absolute magnitude), one sees from Eqs. (22) and (23) that for the CD spectrum the relevant functions are $S(C_{\parallel}) - S(C_{\perp})$ and $S(C_L) - S(C_R)$. For absorption the relevant functions are $\cos^2(\beta)S(C_{\parallel}) + \frac{1}{2}\sin^2(\beta)S(C_{\perp})$ [Eq. (15)] and $S(C_L) + S(C_R) \approx S(C_{\perp})$ [Eq. (20)]. Besides the angle β , only the interaction energies C_{\parallel} , C_{\perp} , and C_{LR} are needed to determine the various line shapes. If we consider, for simplicity, only nearest-neighbor interactions and choose the value of the nearest-neighbor interaction strength to be $V = -750$ cm^{-1} , we have $C_{\parallel} = 2V = -1500$ cm^{-1} , $C_{\perp} = 2V \cos \phi = -1500 \cos \phi$ cm^{-1} , and $C_{RL} = 2V \cos(\phi \mp 0.01) = -1500 \cos(\phi \mp 0.01)$ cm^{-1} . These values are taken in the calculations presented in Fig. 3. To obtain a simple expression for the absorption line shape, the angle β is chosen such that $\sin^2(\beta) = 4 \cos^2(\beta)$; thus $\beta \approx 63^\circ$. Then the line-shape function for light propagating perpendicular to the helix takes the form $S(C_{\parallel}) + 2S(C_{\perp})$. This function is shown in the left column of Figs. 3(b)–3(g) (solid lines) for different angles ϕ . In the same figures also the contribution of light propagating parallel to the helix axis $S(C_{\perp})$ is plotted (dotted line). Because for a given nearest-neighbor interaction strength the value of C_{\parallel} is independent of the angle ϕ , the contribution of $S(C_{\parallel})$, belonging to light polarized parallel to the helix axis, stays the same in all plots (peak centered around 17 800 cm^{-1}). The function $S(C_{\parallel})$ is proportional to the solid curve in Fig. 3(b). In the second column [Figs. 3(h)–3(n)] we have plotted $S(C_{\parallel}) - S(C_{\perp})$ (solid lines), which is proportional to the CD^{perp} , and $S(C_L) - S(C_R)$ (dotted lines), which is proportional to CD^{para} . We will, furthermore, consider the ORD. Therefore, in analogy to Eq. (14), we define

$$R(C) \equiv \text{Re} \frac{\langle g \rangle}{1 - C \langle g \rangle}. \quad (26)$$

In the third column [Figs. 3(p)–3(u)] we have plotted $R(C_{\parallel}) - R(C_{\perp})$ (solid line) and $R(C_L) - R(C_R)$ (dotted line), which are proportional to the ORD of light propagating perpendicular and parallel to the helix axis, respectively.

In the second row [Figs. 3(b), 3(i), and 3(p)], the aggregate spectra in the case $\phi = 0^\circ$, where the dipole transition moments of all monomers are parallel, are displayed. The absorption shows a typical J band (a narrow peak redshifted with respect to the monomer absorption mean position). For

$\phi = 0$, one has $C_{\perp} = C_{\parallel}$, and therefore the position and line shape of the perpendicular polarized absorption band $S(C_{\perp})$ are identical to those of parallel polarization $S(C_{\parallel})$. This is also the reason why the CD spectrum for light propagating perpendicular to the helix axis vanishes [see Eq. (22)]. Since $C_R = C_L$ [see Eq. (19)], the CD spectrum for light polarized parallel to the helix axis vanishes too.

For $\phi = 30^\circ$ [Figs. 3(c), 3(j), and 3(q)], C_{\perp} is slightly bigger than C_{\parallel} and therefore the position of $S(C_{\perp})$ is at higher energies compared to $S(C_{\parallel})$, which leads to an apparent broadening of the J band in the absorption spectrum [Fig. 3(c)] and also to nonvanishing CD and ORD [Figs. 3(j) and 3(q)]. Considering CD^{perp} in Fig. 3(j), one sees that the positive peak [which is due to $S(C_{\parallel})$] is higher and narrower compared to the negative peak [which is due to $S(C_{\perp})$]. This is easy to understand. With increasing C_{\perp} not only is the position of the band $S(C_{\perp})$ shifted to higher energies, but its width also increases, since $|C_{\perp}|$ has decreased.⁵⁷ A similar reasoning holds for CD^{para} .

For $\phi = 60^\circ$ even in the absorption spectrum [Fig. 3(d)] it can be seen that the perpendicular polarized band (centered around 18 500 cm^{-1}) has clearly split off from the parallel polarized band and its width has increased further.

In the case $\phi = 90^\circ$, one has $C_{\perp} = 0$. Thus the line shape $S(C_{\perp})$ is identical to the monomer line shape. This is noteworthy, since if one measures only the isotropic absorption in an experiment, often it is concluded that the broad band from approximately 18 000 to 20 000 cm^{-1} stems from residual monomers. However, CD or ORD can reveal the fact that the band does belong to the same aggregate as the sharp absorption peak at 18 000 cm^{-1} .

With a further increase of ϕ , the energy C_{\perp} becomes positive and, in addition to the parallel polarized J band, a typical H band (blueshifted with respect to the monomer absorption) develops in the aggregate absorption spectrum. The line shape of the H band and the influence of vibrations were extensively studied in Ref. 60. Due to the asymmetric line shape of the monomer, caused by internal vibrations, the line shape $S(C_{\perp})$ of the H band for a given (positive) value of C_{\perp} is not the mirror image of the line shape $S(-C_{\perp})$. In the last row of Fig. 3, the extreme case $\phi = 180^\circ$ (two monomers per turn) is shown. Note that now CD^{perp} vanishes identically [because for $\phi = 180^\circ$, one has $C_R = C_L$, see Eq. (19)].

IV. COMPARISON WITH EXPERIMENT

To apply the foregoing theoretical results to experimental spectra, we consider the absorption and CD spectra of two different dye aggregates, where both monomers show no CD. The first dye to be considered is PIC, whose monomer spectrum has been given already in Fig. 3(a). The second example is the dye 3,3'-bis(3-carboxypropyl)-5,5',6,6'-tetrachloro-1,1'-dioctylbenzimidacarbocyanine (TDBC/C8O3) usually simply abbreviated as C8O3,⁴⁷ which was investigated in some detail recently.^{38–40} Using cryo-transmission electron microscopy, it became possible to resolve the structure of the aggregates of PIC (Ref. 48) and C8O3 (Ref. 49) on the nanometer scale. For PIC a rodlike morphology, with a rod diameter of approximately 2.3 nm,

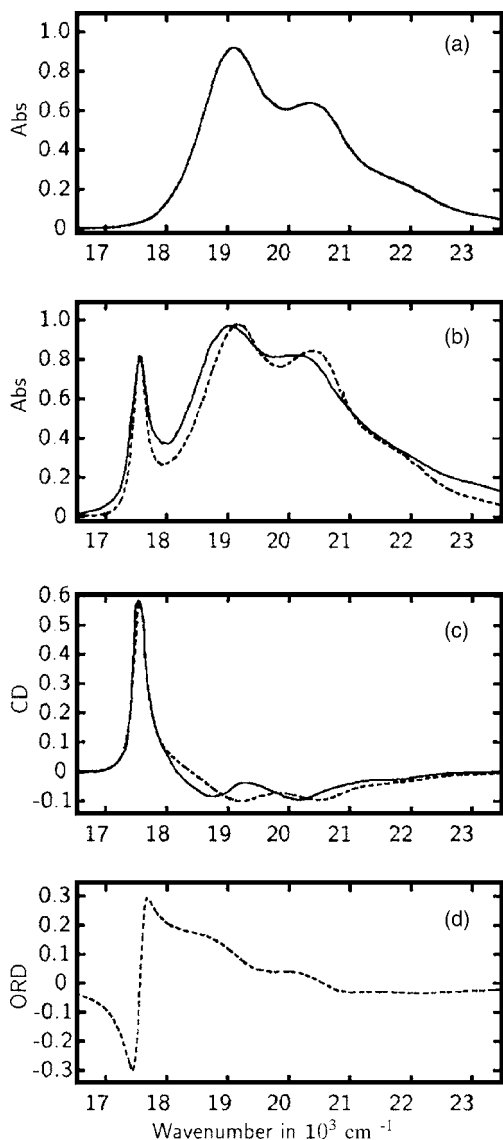


FIG. 4. Comparison of calculated spectra with experiment in the case of PIC. The measured spectra are shown as black solid lines. The dashed lines are the calculated spectra. Monomer absorption (a), aggregate absorption (b), CD (c), and ORD (d). All spectra are in arbitrary units.

has been found.⁴⁸ It was shown that C8O3 aggregates into tubular strands with a diameter of about 10 ± 1 nm (Ref. 49) and that C8O3 (in polyvinyl alcohol) has a bilayered arrangement of the chromophores in the tubulars.³⁹

As demonstrated in the previous section, the measurements of the polarization-dependent absorption spectra and of CD^{para} , CD^{perp} provide important clues to the orientation of the monomers within the cylindrical aggregates. Such studies were carried out by, e.g., Mandel and Holzwarth³⁴ for polypeptides and they were able to extract the various contributions to the CD spectrum corresponding to different light propagation directions.

Unfortunately, we did not find absorption and CD spectra of dye aggregates measured on oriented samples for different light propagation directions. Therefore we can only compare the theory with averaged spectra. For absorption we thus have [see Eq. (21)]

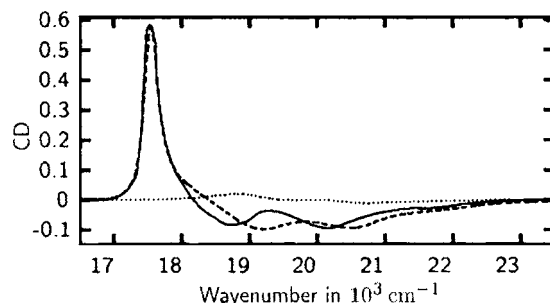


FIG. 5. The two contributions (parallel propagation and perpendicular propagation) to the CD spectrum. The parameters are the same as in the previous figure. Solid line, measured CD. All spectra are in arbitrary units.

$$\sigma^{\text{iso}} \approx F(\cos(\beta)^2 S(C_{\parallel}) + \sin(\beta)^2 S(C_{\perp})). \quad (27)$$

Here $F \equiv 4\pi N \mu^2 \omega / 3c$, $\mu_v^2 = \mu \cos(\beta)^2$, and $(\mu_r^2 + \mu_i^2) = \mu \sin(\beta)^2$ are used (see Fig. 2). Since the distance between neighboring monomers is much smaller than the wavelength of the absorbed light, the approximate Eq. (21) is used. Under this condition ($aq \ll 1$) one can approximate Eq. (19) as follows:

$$C_{R/L} \approx C_{\perp} \pm \Delta, \quad (28)$$

with [see also Eq. (B20)]

$$\Delta = aq \sum_n n_1 \sin(n\phi) V_{n0}. \quad (29)$$

Then the CD spectrum can be written as

$$CD^{\text{iso}} \approx F \left(\frac{\sin(\beta)^2}{2} (S(C_{\perp} - \Delta) - S(C_{\perp} + \Delta)) + \frac{2\pi\rho \sin(2\beta)}{\lambda} \cos(\alpha) (S(C_{\parallel}) - S(C_{\perp})) \right). \quad (30)$$

From Eq. (27) one sees that the isotropic absorption can be fitted using C_{\parallel} , C_{\perp} , and β as fit parameters. Since for the considered dye aggregates the contributions proportional to $S(C_{\parallel})$ and $S(C_{\perp})$ are energetically well separated, from the fit of the aggregate absorption spectrum it is possible to obtain all three parameters C_{\parallel} , C_{\perp} , and β unambiguously. To fit the CD spectrum, one has, furthermore, the parameters α , ρ , and Δ [see Eq. (30)]. Note that the line shape of light propagating parallel to the cylinder axis [second term on the right-hand side (rhs) of Eq. (30)] is already determined by the parameters C_{\parallel} and C_{\perp} obtained from the fit of the absorption spectrum.

A. The pseudoisocyanine dye

Figure 4(a) shows the measured monomer absorption spectrum in methanol.⁶³ The experimental aggregate absorption and CD spectra (solid lines) shown in Fig. 4 are measured in an ethyl cellulose polymer film (5 wt %, $\sim 20 \mu\text{m}$ film thickness).⁶⁴ Measurements on oriented PIC aggregates suggest that the absorption band at around 17500 cm^{-1} is due to the absorption of light that is polarized parallel to the long axis of the aggregates (see, e.g., Ref. 5). Therefore we associate this band with $S(C_{\parallel})$ and the broad band in the region of monomer absorption with $S(C_{\perp})$. As described af-

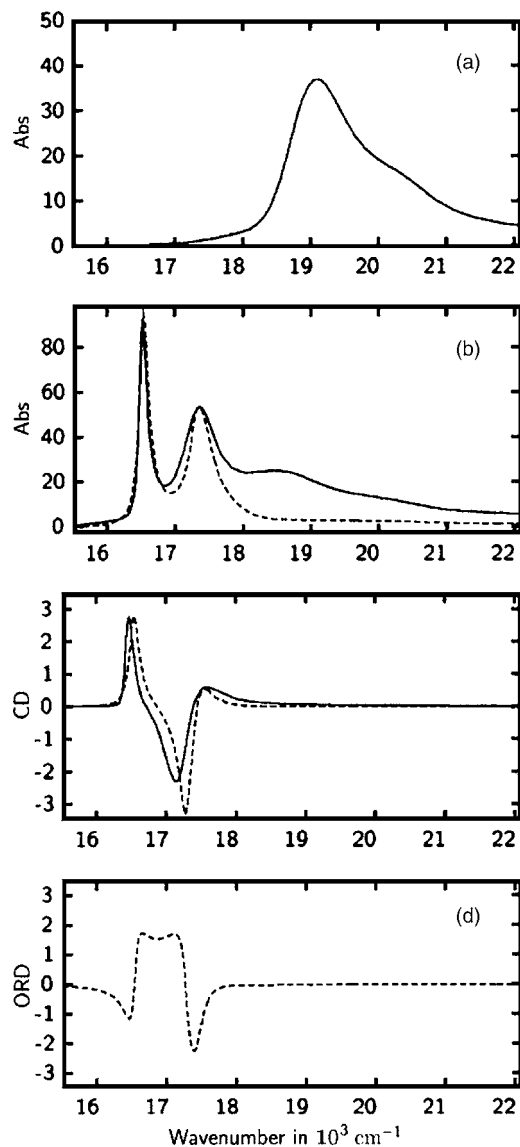


FIG. 6. CD and absorption spectra of C8O3. The measured spectra are shown as black solid lines. The calculated spectra are given by the dotted lines. Monomer absorption (a), aggregate absorption (b), CD (c), and ORD (d). All spectra are in arbitrary units.

ter Eq. (30) from the fit of the aggregate absorption spectrum [Fig. 4(b)], the interaction energies $C_{\parallel} = -1600 \text{ cm}^{-1}$, $C_{\perp} = +180 \text{ cm}^{-1}$, and the angle $\beta = 67^{\circ}$ were obtained.

Next consider the CD spectrum [Fig. 4(c)]. We first fix the parameters of the second term on the rhs of Eq. (30). The line shape is already determined by C_{\parallel} and C_{\perp} . This spectrum is shown in Fig. 5 (dashed line) together with the measured CD (solid line). Since the first term on the rhs of Eq. (30) is centered around $S(C_{\perp})$ and has no contributions in the region of the peak around 17500 cm^{-1} [associated with $S(C_{\parallel})$], the CD signal around 17500 cm^{-1} stems only from the second term on the rhs of Eq. (30). This fact is used to fix the absolute magnitude of $F(2\pi\rho/\lambda)[\sin(2\beta)/2]\cos(\alpha)$. As can be seen in Fig. 5 (dashed line) the contribution so obtained (only light propagating perpendicular to the cylinder) reproduces the CD spectrum quite well. However, there is still the first term on the rhs of Eq. (30) to consider. Using $\Delta = 0,5 \text{ cm}^{-1}$, we found the best agreement between the mea-

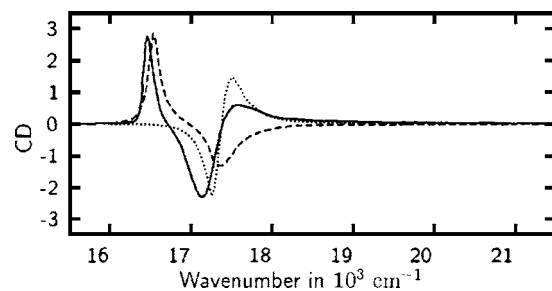


FIG. 7. The two contributions (parallel propagation, dotted; perpendicular propagation, dashed) to the CD spectrum. The parameters are the same as in the previous figure. Solid line, measured CD.

sured CD spectrum and the calculation. The calculated curve can be found in Fig. 4(c) (dashed curve). The contribution of light propagating parallel to the cylinder is shown in Fig. 5 (dotted curve). Due to the fact that the aggregate spectra are measured in a different solvent compared to the monomers, all calculated spectra were slightly shifted to lower energies by 100 cm^{-1} . In Fig. 4(d) the calculated ORD spectrum is shown also. We have found no ORD spectrum measured under similar conditions to the CD and absorption measurements.

B. The C8O3 dye

In Fig. 6 the measured monomer and aggregate spectra of C8O3 are shown as solid lines. The monomer spectrum [Fig. 6(a)] is measured in methanol and the absorption spectrum of the aggregate [Fig. 6(b)] in $10^{-2} M$ NaOH (concentration $5 \times 10^{-4} \text{ mol/l}$). All measured spectra are taken from Ref. 65. The calculation of the theoretical spectra was done in the same way as described in the previous section. Although in Ref. 39 a double cylinder structure was found, we did the fit using the model of a *single* cylinder. From the fit of the absorption spectrum [Fig. 6(b), dashed curve] the parameters $C_{\parallel} = -2800 \text{ cm}^{-1}$, $C_{\perp} = -1930 \text{ cm}^{-1}$, and $\beta = 47^{\circ}$ were obtained. With these parameters the CD spectrum for light propagating perpendicular to the cylinder is fitted as described in the previous section. It is shown in Fig. 7 as the dashed curve. Clearly in the region around $17000\text{--}18000 \text{ cm}^{-1}$ this curve shows little resemblance to the measured spectrum (black solid line). That means there has to be a big contribution from CD^{para} . The best agreement between calculation and measurement was obtained using $\Delta = 17 \text{ cm}^{-1}$. The isotropic CD spectrum fitted in this way is shown in Fig. 6(c). The contribution of light propagating parallel to the cylinder axis is shown in Fig. 7 (dotted curve). One sees a good overall agreement in the absorption spectrum as well as in the CD spectrum of the aggregate. It was shown in Ref. 65 that the peak around 19000 cm^{-1} does not belong to the aggregate but is due to residual monomers, dimers, trimers, etc. We see that in the absorption spectrum the sharp peak at about 16700 cm^{-1} is reproduced very well. The theoretical peak at 17500 cm^{-1} is narrower than the measured one, but that might be due to the above mentioned residual monomers/dimers.

For simplicity, and to minimize the number of fit parameters, the above calculation was based on the assumption of a

single cylindrical aggregate. However, results of cryo-TEM investigations suggest a double cylindrical structure of the C8O3 aggregates with an inner cylinder of diameter ~ 8 nm and an outer cylinder of diameter ~ 12 nm. If one uses two noninteracting cylinders as a model, a larger number of fit parameters is available and accordingly one can achieve better fit results. An example can be found in Ref. 62, where the double cylinder model suggested by the cryo-TEM investigations is adopted and almost perfect agreement between theory and experiment are obtained, although, as mentioned before, the Rosenfeld approach is used. The formulas derived for isotropic samples with the formalism used in Ref. 62 are equivalent to the results reported in this paper for the case of cylinders with their axis oriented perpendicular to the light propagation direction. Note that in the fit shown in Fig. 6 there is a contribution of parallel propagating light that can not be ignored (see Fig. 7).

V. CONCLUSIONS

In this paper the absorption and CD of infinite cylindrical molecular aggregates are studied. Using the CES approximation to handle internal vibrations of the monomers, simple expressions for the absorption and CD spectra of the aggregate are derived which demonstrate clearly the dependence of the spectra on the propagation direction of the absorbed light with respect to the axis of the cylinder. A theoretical consideration in the special case of a helical aggregate showed that the spectra exhibit a strong dependence on the number of monomers per turn. It might be interesting to study in the CES approximation finite helical/cylindrical aggregates and compare the results, on the one hand, with the infinite case considered in this paper and, on the other hand, with spectra obtained from an exact diagonalization of the aggregate Hamiltonian (which we find can only be accomplished for aggregates consisting of not more than approximately ten monomers if one includes one vibrational mode).

A comparison between theoretical calculations and experimental spectra gives good agreement when fitting both the absorption and the CD spectra simultaneously. However, it was not possible to deduce the molecular arrangement (position and orientation of the monomers) within the cylinder, since no experimental spectra for different light propagation directions are available. The possibility to extract all parameters necessary to specify the geometry will now be discussed briefly. The parameters of the cylindrical aggregate are (see Fig. 2) ϕ_1 , ϕ_2 , a , ρ , α , and β . The parameters used to fit the spectra are C_{\parallel} , C_{\perp} , Δ , ρ , α , and β . As discussed in Sec. IV, from the fit of the absorption spectra one can obtain

C_{\parallel} , C_{\perp} , and β . The fit of CD^{para} then yields Δ (here we have used that if the wavelength of light is much longer than the distance between neighboring monomers, one can write $C_{L/R} = C_{\perp} \mp \Delta$). To fit CD^{perp} only the radius ρ and the angle α are left as free fit parameters. For a known radius (e.g., from cryo-TEM measurements), fitting of propagation dependent absorption and CD spectra yields the parameters C_{\parallel} , C_{\perp} , $C_{L/R}$, α , and β . The angles α and β determine the orientation of the monomers in the cylinder. The energies C_{\parallel} , C_{\perp} , and $C_{L/R}$ depend explicitly and also implicitly on ϕ_1 , ϕ_2 , and a via the dipole-dipole interaction

$$V_{nm} \propto \frac{\boldsymbol{\mu}_n \cdot \boldsymbol{\mu}_m - 3\boldsymbol{\mu}_n \cdot (\mathbf{X}_m - \mathbf{X}_n)\boldsymbol{\mu}_m \cdot (\mathbf{X}_m - \mathbf{X}_n)}{|\mathbf{X}_m - \mathbf{X}_n|^3}. \quad (31)$$

Thus, in principle, it is possible to solve the system of equations given by Eqs. (17)–(19) to obtain ϕ_1 , ϕ_2 , and a . This consideration shows that the use of oriented samples with orientations parallel and perpendicular with respect to the propagation direction of the light beam would allow the precise geometrical arrangement of the monomers to be inferred from the measurement. This is not possible using only the data on the isotropic case.

ACKNOWLEDGMENT

Financial support of the DFG in the Project Br 728/11 is acknowledged gratefully.

APPENDIX A: THE CYLINDRICAL GEOMETRY

In the cylindrical geometry described in Sec. III, the position of monomer n is given by

$$\mathbf{X}_n = \begin{pmatrix} \rho \cos \theta \cos n\phi - \rho \sin \theta \sin n\phi \\ \rho \sin \theta \cos n\phi + \rho \cos \theta \sin n\phi \\ hn_1 \end{pmatrix}. \quad (A1)$$

We have introduced the angle θ which allows for a rotation around the cylinder axis. (We will average over this angle when we calculate the CD for light propagating perpendicular to the cylinder axis.) If $\mu_r \equiv \mu \sin \beta \sin \alpha$, $\mu_t \equiv \mu \sin \beta \cos \alpha$, and $\mu_v \equiv \mu \cos \beta$ (α and β are defined in Fig. 2) are used to specify the radial, tangential, and vertical (parallel to the cylinder axis) components of the transition dipole located in the zero residue, then the transition dipole of monomer n is given by³²

$$\boldsymbol{\mu}_n = \frac{1}{2} \begin{pmatrix} e^{-in\phi}(\mu_r - i\mu_t)(\cos \theta - i \sin \theta) + e^{in\phi}(\mu_r + i\mu_t)(\cos \theta + i \sin \theta) \\ e^{-in\phi}(\mu_r - i\mu_t)(\sin \theta + i \cos \theta) + e^{in\phi}(\mu_r + i\mu_t)(\sin \theta - i \cos \theta) \\ 2\mu_v \end{pmatrix}. \quad (A2)$$

APPENDIX B: DERIVATION OF THE ABSORPTION AND CD SPECTRA

In this appendix expressions for the CD spectra of cylindrical aggregates will be derived. First we consider light that is propagating perpendicular to the cylinder axis and then the case of light propagating parallel to the cylinder axis. The treatment of the two cases is slightly different: as outlined in Sec. I, in the first case the Rosenfeld treatment can be used; in the second case, this approximation is not justified.

1. CD for light propagating perpendicular to the cylinder axis

Consider light propagating in the x direction. (The cylinder axis is parallel to the z axis.) The wave vector \mathbf{q} is then given by $\mathbf{q} = q\hat{e}_x$, and the polarization vector for right and left circularly polarized light is $\boldsymbol{\varepsilon}_{R/L} = (1/\sqrt{2})(\hat{e}_y \mp i\hat{e}_z)$. To obtain the CD signal for this propagation direction, we will first rewrite Eq. (11) using the cylinder geometry described in the Appendix A. To find the CD in terms of the monomer bandshape function, we will then apply the CES approximation to handle the nuclear degrees of freedom of the monomers. We will make use of the fact that the radius of the helices is small compared to the wavelength of light, so that it is enough to expand the exponential containing the factor $i\mathbf{q} \cdot (\mathbf{X}_m - \mathbf{X}_n)$ only to first order, which corresponds to the standard Rosenfeld treatment.

Let us begin by rewriting Eq. (11). Inserting Eq. (10) into Eq. (11) and using Eq. (A2), we obtain

$$\text{CD}_{q=q\hat{e}_x} = -\frac{4\pi}{c} \omega \text{Im} \sum_{nm} \langle G_{nm} \rangle [(\boldsymbol{\varepsilon}_L \cdot \boldsymbol{\mu}_n)^* (\boldsymbol{\mu}_m \cdot \boldsymbol{\varepsilon}_L) - (\boldsymbol{\varepsilon}_R \cdot \boldsymbol{\mu}_n)^* (\boldsymbol{\mu}_m \cdot \boldsymbol{\varepsilon}_R)] e^{iq\hat{e}_x \cdot (\mathbf{X}_m - \mathbf{X}_n)}. \quad (\text{B1})$$

For different orientations of the cylinder (described by the rotation angle θ), the CD is, in general, different. We are only interested in the CD averaged over all rotations of the cylinder about its axis,

$$\text{CD}^{\text{perp}} = \int_0^{2\pi} d\theta w(\theta) \text{CD}_{q\hat{e}_x}(\theta), \quad (\text{B2})$$

with $w(\theta)$ the probability to find the cylinder rotated by an angle θ around the (long) cylinder axis. If we assume equal probabilities for all angles, e.g., $w(\theta) = 1/2\pi$, then we obtain

$$\text{CD}^{\text{perp}} = -\frac{4\pi}{c} \omega \text{Im} \sum_{nm} \langle G_{nm} \rangle \int_0^{2\pi} \frac{d\theta}{2\pi} \times [(\boldsymbol{\varepsilon}_L \cdot \boldsymbol{\mu}_n)^* (\boldsymbol{\mu}_m \cdot \boldsymbol{\varepsilon}_L) - (\boldsymbol{\varepsilon}_R \cdot \boldsymbol{\mu}_n)^* (\boldsymbol{\mu}_m \cdot \boldsymbol{\varepsilon}_R)] e^{iq\hat{e}_x \cdot (\mathbf{X}_m - \mathbf{X}_n)}. \quad (\text{B3})$$

If the radius ρ is small compared to the wavelength of the incoming light, we can make the approximation $e^{iq\hat{e}_x \cdot (\mathbf{X}_m - \mathbf{X}_n)} \approx 1 + iq\hat{e}_x \cdot (\mathbf{X}_m - \mathbf{X}_n)$. Performing the integration in Eq. (B3) and using Eq. (A1), we find

$$\text{CD}^{\text{perp}} = -\frac{4\pi}{c^2} \omega^2 \mu_r \mu_v \rho \times \text{Im} \sum_{nm} \langle G_{nm}(E) \rangle (1 - \cos[(m-n)\phi]), \quad (\text{B4})$$

where $q = \omega/c$ is used.

To proceed further, we use the identity Eq. (13) in the CES approximation. First we consider the term $\sum_{nm} \langle G_{nm}(E) \rangle$ in Eq. (B4) and obtain

$$\sum_{nm} \langle G_{nm} \rangle - \langle g \rangle \sum_{n'n'm} V_{n'n'} \langle G_{n'm} \rangle = \sum_n \langle g \rangle, \quad (\text{B5})$$

where we have also assumed that V is independent of the vibrational averaging. For an infinite one-dimensional aggregate, it is easy to see that

$$\sum_n V_{n'n'} \equiv C_{\parallel} \quad (\text{B6})$$

is independent of n' . Using Eqs. (17) and (B5) we obtain

$$\sum_{nm} \langle G_{nm} \rangle - \langle g \rangle C_{\parallel} \sum_{n'm} \langle G_{n'm} \rangle = N \langle g \rangle \quad (\text{B7})$$

and solve for $\sum_{nm} \langle G_{nm} \rangle$ to obtain

$$\sum_{nm} \langle G_{nm} \rangle = N \frac{\langle g \rangle}{1 - C_{\parallel} \langle g \rangle}. \quad (\text{B8})$$

This is the first contribution to the CD spectrum of the cylinder for light propagating perpendicular to the cylinder axis. As shown in Ref. 59 the right-hand side of Eq. (B8) is the line shape for *absorption* of light polarized parallel to the cylinder axis. This explains the designation C_{\parallel} .

For the second contribution in Eq. (B4) we have to calculate $\sum_{nm} \langle G_{nm}(E) \rangle \cos[(m-n)\phi]$. We proceed analogously to the derivation of Eq. (B8) and obtain, within the CES approximation,

$$\sum_{nm} \langle G_{nm}(E) \rangle \cos[(m-n)\phi] = N \frac{\langle g \rangle}{1 - C_{\perp} \langle g \rangle}, \quad (\text{B9})$$

where we have introduced

$$\sum_n V_{n'n'} \cos[(n' - n)\phi] \equiv C_{\perp}. \quad (\text{B10})$$

Equation (B9) is the line shape for absorption of light polarized perpendicular to the cylinder axis. Inserting Eqs. (B9) and (B8) into Eq. (B4) we obtain finally

$$\text{CD}^{\text{perp}} = -\frac{4\pi N}{c^2} \omega^2 \mu_r \mu_v \rho \text{Im} \left(\frac{\langle g \rangle}{1 - C_{\parallel} \langle g \rangle} - \frac{\langle g \rangle}{1 - C_{\perp} \langle g \rangle} \right). \quad (\text{B11})$$

2. CD for light propagating parallel to the cylinder axis

For light propagating in the z direction (along the cylinder axis), the wave vector \mathbf{q} is given by $\mathbf{q} = q\hat{e}_z$ and the polarization vector for right and left polarized light is $\boldsymbol{\varepsilon}_{R/L} = (1/\sqrt{2})(\hat{e}_x \mp i\hat{e}_y)$.

In this case of light propagating parallel to the cylinder axis, it is possible to obtain the absorption spectra for left

and right circularly polarized light without any further approximation (apart from the CES approximation). We will therefore proceed differently as in the previous section (CD for light propagating perpendicular to the cylinder axis), where we expanded the factor $\exp(-iq \cdot X_n)$ to first order. Now we cannot make this expansion because the length of the cylinder is much longer than the wavelength of the light. Therefore we have to keep the whole factor $\exp(-iq \cdot X_n) = \exp(-iqan_1)$.

Starting from Eq. (10) and using the identity Eq. (13) in the CES approximation, one obtains

$$\begin{aligned} & \sum_{nm} \boldsymbol{\varepsilon}_{R/L}^* \cdot \boldsymbol{\mu}_n e^{-iqan_1} \langle G_{nm} \rangle \boldsymbol{\varepsilon}_{R/L} \cdot \boldsymbol{\mu}_m e^{iqam_1} \\ & - \langle g \rangle \sum_{nmn'} \boldsymbol{\varepsilon}_{R/L}^* \cdot \boldsymbol{\mu}_n e^{-iqan_1} V_{nn'} \langle G_{n'm} \rangle \boldsymbol{\varepsilon}_{R/L} \cdot \boldsymbol{\mu}_m e^{iqam_1} \\ & = \sum_{nm} \langle g_n \rangle \delta_{nm} \boldsymbol{\varepsilon}_{R/L}^* \cdot \boldsymbol{\mu}_n e^{-iqan_1} \boldsymbol{\varepsilon}_{R/L} \cdot \boldsymbol{\mu}_m e^{iqam_1}. \end{aligned} \quad (\text{B12})$$

The first term on the left-hand side is proportional to the absorption spectrum of the aggregate for light that is propagating parallel to the cylinder axis and is right or left circularly polarized. The term of the right-hand side is proportional to the absorption spectrum of the monomers. We consider the second term on the left-hand side of Eq. (B12) and define

$$C_{R/L} \equiv \sum_n e^{i(\pm\phi(n-n')-qa(n_1-n'_1))} V_{nn'}, \quad (\text{B13})$$

which is independent of n' . Then one finds that

$$\sum_{nmn'} \boldsymbol{\varepsilon}_{R/L}^* \cdot \boldsymbol{\mu}_n e^{-iqan_1} V_{nn'} = C_{R/L} \sum_{n'} \boldsymbol{\varepsilon}_{R/L}^* \cdot \boldsymbol{\mu}_{n'} e^{-iqan'_1} \quad (\text{B14})$$

and the left-hand side (LHS) of Eq. (B12) becomes

$$\begin{aligned} \text{LHS} & = (1 - C_{R/L} \langle g \rangle) \sum_{n'm} \boldsymbol{\varepsilon}_{R/L}^* \boldsymbol{\mu}_{n'} e^{-iqan'_1} \\ & \times \langle G_{n'm} \rangle \boldsymbol{\varepsilon}_{R/L} \cdot \boldsymbol{\mu}_m e^{iqam_1}. \end{aligned} \quad (\text{B15})$$

Denoting the absorption spectrum for left and right circularly polarized light with wave vector $\mathbf{q} = q\hat{e}_z$ by $\sigma_{q\hat{e}_z}^{R/L}(\omega)$, one has

$$\begin{aligned} \sigma_{q\hat{e}_z}^{R/L}(\omega) & = -\frac{4\pi}{c} \omega \text{Im} \sum_{nm} \boldsymbol{\varepsilon}_{R/L}^* \cdot \boldsymbol{\mu}_n e^{-iqan_1} \\ & \times \langle G_{nm} \rangle \boldsymbol{\varepsilon}_{R/L} \cdot \boldsymbol{\mu}_m e^{iqam_1}, \end{aligned} \quad (\text{B16})$$

and using the results Eqs. (B15) and (B12), one obtains

$$\sigma_{q\hat{e}_z}^{R/L}(\omega) = -\frac{4\pi N}{c} \omega \frac{(\mu_r^2 + \mu_t^2)}{2} \text{Im} \frac{\langle g \rangle}{1 - C_{R/L} \langle g \rangle}. \quad (\text{B17})$$

Using the definition of CD [Eq. (11)] one directly obtains the CD for light propagating parallel to the cylinder axis as

$$\begin{aligned} \text{CD}^{\text{para}} & = -\frac{4\pi N}{c} \omega \frac{(\mu_r^2 + \mu_t^2)}{2} \\ & \times \text{Im} \left[\frac{\langle g \rangle}{1 - C_L \langle g \rangle} - \frac{\langle g \rangle}{1 - C_R \langle g \rangle} \right]. \end{aligned} \quad (\text{B18})$$

To compare our results with those of previous theories, we will make some further approximations. First note that

$$C_L - C_R = -4 \sum_{n_1 > 0} \sum_{n_2=0}^{N_2-1} \sin(n\phi) \sin(qan_1) V_{n0}. \quad (\text{B19})$$

For molecular aggregates typically $a \approx 1$ nm and $1/q \approx 100$ nm, so that one can expand $\sin(qan_1)$ in Eq. (B19) to obtain

$$C_L - C_R \approx -4qa \sum_{n_1 > 0} \sum_{n_2=0}^{N_2-1} n_1 \sin(n\phi) V_{n0}. \quad (\text{B20})$$

In making this expansion one has to be careful, since for large n_1 the argument qan_1 becomes also large. However, for large n_1 the interaction V_{n0} becomes very small, so that the expansion can be performed. Formally one can introduce a cutoff n_1^{max} in the n_1 summation. A consideration similar to the one above was used by Loxsom³¹ to compare his results with those of Moffitt *et al.*¹⁵ With the result Eq. (B20) we can rewrite Eq. (B18) as

$$\begin{aligned} \text{CD}^{\text{para}} & \approx -\frac{4\pi N}{c} \omega \frac{(\mu_r^2 + \mu_t^2)}{2} \\ & \times \text{Im} \left[(C_L - C_R) \frac{\langle g \rangle^2}{(1 - C_{\perp} \langle g \rangle)^2} \right] \\ & \approx -\frac{8\pi N}{c} \omega (\mu_r^2 + \mu_t^2) \\ & \times \left(-qa \sum_{n_1 > 0} \sum_{n_2} n_1 \sin(n\phi) \right) \\ & \times \text{Im} \left[\frac{\langle g \rangle^2}{(1 - C_{\perp} \langle g \rangle)^2} \right]. \end{aligned} \quad (\text{B21})$$

In the first step we have used in the denominator $C_R \approx C_L \approx C_{\perp}$.

Using $(\partial/\partial\omega)\langle g \rangle = -\hbar\langle g \rangle^2$, one finds $\text{Im}\langle g \rangle^2/(1 - C_{\perp}\langle g \rangle)^2 = (1/\hbar)(\partial/\partial\omega)S(C_{\perp})$ with $S(C_{\perp}) = -\text{Im}[\langle g \rangle/(1 - C_{\perp}\langle g \rangle)]$ the absorption line shape of light polarized perpendicular to the cylinder axis [see Eq. (14)]. Thus

$$\begin{aligned} \text{CD}^{\text{para}} & \approx \frac{4\pi N}{c} \omega (\mu_r^2 + \mu_t^2) \left(qa \sum_n n_1 \sin(n\phi) V_{n0} \right) \\ & \times \frac{\partial}{\partial(\hbar\omega)} S(C_{\perp}, \omega), \end{aligned} \quad (\text{B22})$$

which shows that the line shape of the CD band for light propagating parallel to the cylinder axis is approximately the derivative of the corresponding absorption line shape for light polarized perpendicular to the cylinder axis. This is in accordance with the results given in Refs. 23, 32, 34, and 46.

¹A. E. Hansen, Adv. Chem. Phys. **44**, 545 (1980).

²A. Rodger and B. Nordén, *Circular Dichroism and Linear Dichroism* (Oxford University Press, New York, 1997).

³H. van Amerongen, L. Valkunas, and R. van Grondelle, *Photosynthetic Excitons* (World Scientific, Singapore, 2000).

⁴S. Georgakopoulou, R. van Grondelle, and G. van der Zwan, J. Phys. Chem. B **110**, 3344 (2006).

- ⁵ *J-Aggregates*, edited by T. Kobayashi (Word Scientific, Singapore, 1996).
- ⁶ A. Sanchez-Castillo, C. E. Roman-Velazquez, and C. Noguez, *Phys. Rev. B* **73**, 045401 (2006).
- ⁷ C. E. Román-Velázquez, C. Noguez, and I. L. Garzón, *J. Phys. Chem. B* **107**, 12035 (2003).
- ⁸ S. Sforza, E. Scaravelli, R. Corradini, and R. Marchelli, *Chirality* **17**, 515 (2005).
- ⁹ F. D. Lewis, L. G. Zhang, X. Y. Liu, X. B. Zuo, D. M. Tiede, H. Long, and G. C. Schatz, *J. Am. Chem. Soc.* **127**, 14445 (2005).
- ¹⁰ E. U. Condon, *Rev. Mod. Phys.* **9**, 432 (1937).
- ¹¹ A. Moscowitz, *Adv. Chem. Phys.* **4**, 67 (1962).
- ¹² D. J. Caldwell and H. Eyring, *The Theory of Optical Activity* (Wiley, New York, 1971).
- ¹³ J. G. Kirkwood, *J. Chem. Phys.* **5**, 479 (1937).
- ¹⁴ W. Moffitt, *J. Chem. Phys.* **25**, 467 (1956).
- ¹⁵ W. Moffitt, D. D. Fitts, and J. G. Kirkwood, *Proc. Natl. Acad. Sci. U.S.A.* **43**, 723 (1957).
- ¹⁶ I. Tinoco and R. W. Woody, *J. Chem. Phys.* **32**, 461 (1960).
- ¹⁷ I. J. Tinoco, *Adv. Chem. Phys.* **4**, 113 (1962).
- ¹⁸ A. D. McLachlan and M. A. Ball, *Mol. Phys.* **8**, 581 (1964).
- ¹⁹ H. DeVoe, *J. Chem. Phys.* **43**, 3199 (1965).
- ²⁰ M. R. Philpott, *J. Chem. Phys.* **56**, 683 (1972).
- ²¹ H. Ito, T. Eri, and Y. J. I'Haya, *Chem. Phys. Lett.* **39**, 150 (1976).
- ²² D. A. Rabenold, *J. Chem. Phys.* **74**, 941 (1981).
- ²³ H. O. Pamuk, A. M. Dougherty, and W. C. Johnson, *Biopolymers* **24**, 1337 (1985).
- ²⁴ D. A. Rabenold and W. Rhodes, *Biopolymers* **26**, 109 (1987).
- ²⁵ R. A. Harris, *J. Chem. Phys.* **43**, 959 (1965).
- ²⁶ W. Rhodes, *J. Chem. Phys.* **53**, 3650 (1970).
- ²⁷ R. P. Hemenger, *J. Chem. Phys.* **68**, 1722 (1978).
- ²⁸ M. Kamiya, *Chem. Phys. Lett.* **96**, 569 (1983).
- ²⁹ L. Rosenfeld, *Z. Phys.* **52**, 161 (1928).
- ³⁰ T. Ando, *Prog. Theor. Phys.* **40**, 471 (1968).
- ³¹ F. M. Loxsom, *J. Chem. Phys.* **51**, 4899 (1969).
- ³² C. W. Deutsche, *J. Chem. Phys.* **52**, 3703 (1970).
- ³³ F. M. Loxsom, *Phys. Rev. B* **1**, 858 (1969).
- ³⁴ R. Mandel and G. Holzwarth, *J. Chem. Phys.* **57**, 3469 (1972).
- ³⁵ L. Stryer and E. R. Blout, *J. Am. Chem. Soc.* **83**, 1411 (1961).
- ³⁶ M. R. Philpott, *J. Chem. Phys.* **55**, 4005 (1971).
- ³⁷ O. J. G. Somsen, R. van Grondelle, and H. van Amerongen, *Biophys. J.* **71**, 1934 (1996).
- ³⁸ C. Spitz, J. Knoester, A. Ouart, and S. Dähne, *Chem. Phys.* **275**, 271 (2002).
- ³⁹ H. von Berlepsch, S. Kirstein, R. Hania, C. Didraga, A. Pugžlys, and C. Böttcher, *J. Phys. Chem. B* **107**, 14176 (2003).
- ⁴⁰ C. Spitz, S. Dähne, A. Ouart, and H. W. Abraham, *J. Phys. Chem. B* **104**, 8664 (2000).
- ⁴¹ J. L. Seifert, R. E. Connor, S. A. Kushon, M. Wang, and B. A. Armitage, *J. Am. Chem. Soc.* **121**, 2987 (1999).
- ⁴² M. Bednarz and J. Knoester, *J. Phys. Chem. B* **105**, 12913 (2001).
- ⁴³ S. Dähne, *Bunsen-Magazin* **4**, 81 (2002).
- ⁴⁴ V. I. Prokhorenko, D. B. Steensgaard, and A. R. Holzwarth, *Biophys. J.* **85**, 3173 (2003).
- ⁴⁵ C. Didraga and J. Knoester, *J. Lumin.* **102**, 60 (2003).
- ⁴⁶ C. Didraga, J. A. Klugkist, and J. Knoester, *J. Phys. Chem. B* **106**, 11474 (2002).
- ⁴⁷ C. Didraga, A. Pugžlys, P. R. Hania, H. von Berlepsch, K. Duppen, and J. Knoester, *J. Phys. Chem. B* **108**, 14976 (2004).
- ⁴⁸ H. von Berlepsch, C. Böttcher, and L. Dähne, *J. Phys. Chem. B* **104**, 8792 (2000).
- ⁴⁹ H. von Berlepsch, C. Böttcher, A. Ouart, C. Burger, S. Dähne, and S. Kirstein, *J. Phys. Chem. B* **104**, 5255 (2000).
- ⁵⁰ P. O. J. Scherer and S. F. Fischer, *Chem. Phys.* **86**, 269 (1984).
- ⁵¹ R. P. Hemenger, *J. Chem. Phys.* **66**, 1795 (1977).
- ⁵² J. S. Briggs and A. Herzenberg, *Mol. Phys.* **21**, 865 (1971).
- ⁵³ P. Herman, U. Kleinekatehöfer, I. Barvík, and M. Schreiber, *J. Lumin.* **94**, 447 (2001).
- ⁵⁴ E. W. Knapp, *Chem. Phys.* **85**, 73 (1984).
- ⁵⁵ V. A. Malyshev, *J. Lumin.* **55**, 225 (1993).
- ⁵⁶ J. Schütze, B. Brüggemann, T. Renger, and V. May, *Chem. Phys.* **275**, 333 (2002).
- ⁵⁷ A. Eisfeld and J. S. Briggs, *Phys. Rev. Lett.* **96**, 113003 (2006).
- ⁵⁸ J. S. Briggs and A. Herzenberg, *J. Phys. B* **3**, 1663 (1970).
- ⁵⁹ A. Eisfeld and J. S. Briggs, *Chem. Phys.* **281**, 61 (2002).
- ⁶⁰ A. Eisfeld and J. S. Briggs, *Chem. Phys.* **324**, 376 (2006).
- ⁶¹ J. S. Briggs, Ph.D. thesis, Victoria University of Manchester, 1968.
- ⁶² R. Kniprath, Diplomarbeit, Universität Freiburg, 2004.
- ⁶³ B. Neumann, *J. Phys. Chem. B* **105**, 8268 (2001).
- ⁶⁴ F. D. Saeva and G. R. Olin, *J. Am. Chem. Soc.* **99**, 4848 (1977).
- ⁶⁵ C. Spitz, Ph.D. thesis, Freie Universität Berlin, 1999.